



Aerocapture Trajectories for Spacecraft with Large, Towed Ballutes

Jeffery L. Hall and Andrew K. Le

**Jet Propulsion Laboratory
California Institute of Technology
Pasadena, CA, 91109**

AAS/AIAA Space Flight Mechanics Meeting

Santa Barbara, California

11-15 February 2001

AAS Publications Office, P.O. Box 28130, San Diego, CA 92198

AEROCAPTURE TRAJECTORIES FOR SPACECRAFT WITH LARGE, TOWED BALLUTES

Jeffery L. Hall and Andrew K. Le

Large, towed inflatable structures called ballutes are a potential technology for enabling aerocapture maneuvers of spacecraft at other planets. The ballute provides most of the drag force and energy dissipation during the maneuver and is detached once the desired velocity change has been achieved. A key premise of this concept is that the timing of ballute detachment provides sufficient trajectory modulation capability to enable aerocapture despite atmospheric uncertainties and navigation errors at the target planet. Numerical simulations performed by two independent computer programs for four candidate missions have confirmed this premise and quantified the entry corridor in terms of initial flight path angle and zero-drag periapsis altitude ranges at each planet. A shared result across these missions is that the zero-drag periapse altitude range divided by the density scale height of the atmosphere yields a common value of approximately 2 despite a wide range of entry velocities, spacecraft masses and atmospheric compositions. Another important shared feature is that the aerocapture heating pulse is of short duration with a maximum value of approximately 250 seconds for the most challenging mission.

INTRODUCTION

A ballute is an inflatable structure used to increase the drag of the vehicle to which it is attached. It is very much like a parachute in this respect and primarily differs by having a closed shape that can be inflated with vehicle-supplied gas to deploy in very low pressure or vacuum environments. Also, the inflation pressure can be made high enough to provide appreciable stiffness to the ballute membrane, thereby enabling non-parachute shapes like cones, toroids and spheres. A ballute is typically stored in a container for the initial segment of the parent vehicle's flight, then deployed and inflated at the moment the additional drag is required for trajectory modulation purposes. The ballute either stays with the vehicle to the end of the flight or it is detached after the desired vehicle deceleration has been achieved. Numerous earth and space applications for ballutes have been identified over the years, including stabilization and deceleration of aircraft-delivered bombs,¹ de-orbiting low earth orbit satellites,² supersonic deceleration of Mars

landers³ and aerocapture into orbit around other planets.⁴ Although both earth applications have seen successful prototype flights, no planetary ballute has ever flown.

Aerocapture is a maneuver in which a spacecraft flies through another planet's atmosphere and uses the resulting drag to decelerate into orbit. The key advantage of this maneuver is that it can save considerable fuel mass versus the alternative of propulsive orbit insertion. For example, the 1990 Magellan spacecraft to Venus burned 2000 kg of solid propellant out of a total vehicle mass of 3400 kg (59% mass fraction) to achieve an 0.4 eccentricity orbit. Even larger mass fractions are required if circular orbits and/or high velocity missions are involved. The price of using an aerocapture maneuver to save fuel is that additional spacecraft mass is required for the drag structure and for thermal and pressure protection during hypersonic flight through the atmosphere. Also, one must solve the guidance and control problem to ensure that the spacecraft achieves the desired orbit in the face of approach navigation errors and atmospheric uncertainties. The combination of these difficulties has been sufficient to slow development of aerocapture technology and prevent any prototype flights to date.

Recent interest in developing aerocapture technology stems from the changing character of NASA's solar system exploration program. Fly-by missions are giving way to orbiter, in situ and sample return missions, and many of those require spacecraft in low, circular orbits for telecommunications relay or sample rendezvous and collection. Table 1 lists five future missions described in the current space science strategic plan that require the propellant mass savings afforded by aerocapture.⁵ Also listed are target values for aerocapture system masses once the technology has been developed. As can be seen, the potential fuel savings are enormous and promise to greatly reduce the cost of launch vehicles.

There are two leading candidates for aerocapture technology: maneuverable aeroshells and ballutes. Maneuverable aeroshells are the more mature of the two options and consist of rigid, blunt-body enclosures for the spacecraft adapted from entry capsule technology. In this case, the drag and thermal protection functions are combined into a single aeroshell structure. Unlike entry capsules, aerocapture aeroshells require a small lift coefficient to sufficiently modulate the atmospheric portion of the trajectory. Recent simulations for Mars aerocapture suggest that a lower limit of $C_L \sim 0.25$ is required to compensate for navigational and atmospheric uncertainties and successfully achieve orbit.⁶ One drawback of this technology is that the aeroshell completely encloses the vehicle and therefore interferes with telecommunications, thermal management, on board navigation and solar power collection. The preliminary design of a Mars aerocapture vehicle by CNES sought to finesse this problem by using a front shell but no back shell.⁷ The feasibility of this approach is under active investigation.

Table 1: Comparison of Propulsion and Aerocapture Options for Future Missions

Mission Name	Mission Characteristics				Propulsive Option		Aerocapture Option	
	Entry speed (km/s)	Target orbit (km)	Orbit insert. DV (km/s)	Non-braking mass delivered to orbit (kg)	Propellant mass for orbit insertion ¹ (kg)	Propellant mass fraction	Desired system mass (kg)	Desired system mass fraction
Mars Comm/Nav Sat	6.4	600 circ	2.9	100	170	63%	25	20%
Venus Sample Return	11.6	300 circ	4.5	2600	9200	78%	1100	30%
Titan Explorer	9.6	1000 circ	8.0	325	4100	93%	140	30%
Saturn Ring Observer	26.1	56000 circ	8.0	250	3300	93%	1000	40%
Neptune Orbiter	28.9	500000 ell	5.9	230	1400	86%	150	40%

¹ Assumes Isp = 300 s

In contrast to aeroshells, aerocapture ballutes derive minimal heritage from existing space technology and are at an early stage of development. Nevertheless, the emerging designs suggest the possibility of lighter-weight systems than aeroshells with greatly simplified guidance and control requirements, and avoidance of complete spacecraft enclosures with all of the attendant interference problems. The key difficulty in using inflatable structures for aerocapture is the temperature limitation of flexible, gas-tight membrane materials. Temperatures of thousands of degrees are typically experienced by atmospheric entry capsules, values far in excess of any known ballute (balloon) material. It is therefore essential to substantially decrease the peak heating in order to use inflatable structures. One way to do this is to greatly reduce the ballistic coefficient, B , of the overall vehicle:

$$B = \frac{M}{C_D A} \quad (1)$$

where M is the total mass of the vehicle, C_D is the drag coefficient and A is the cross section area presented to the flow. Recent calculations have demonstrated that vehicles with a lower B fly less deeply into a planet's atmosphere than a higher B vehicle to achieve the same velocity change.^{8,9,10} The difference in minimum altitude can be many scale heights of the planetary atmosphere, corresponding to a few orders of magnitude reduction in peak density experienced by the vehicle. This has two important consequences: first, the peak dynamic pressure on the vehicle reduces by the same few orders of magnitude (dynamic pressure scales with density); and second, the peak heating per unit area, \dot{Q} , decreases significantly according to the standard equation for stagnation point convective heating on a blunt body:

$$\dot{Q} = C \sqrt{\frac{\rho}{R_{cur}}} V^3 \quad (2)$$

where C is a constant, ρ is the atmospheric density, R_{cur} is the radius of curvature at the stagnation point, and V is the vehicle velocity. Equation 2 contains another important clue to the emerging ballute solution, namely that heating scales with $R_{cur}^{-0.5}$ and therefore large ballutes have inherently smaller stagnation point heating rates. This reinforces the message from Equation 1 in which we want a large ballute anyway to increase the cross-sectional area and decrease the ballistic coefficient. The fact that these large ballutes will experience very low dynamic pressures during aerocapture is an important aspect that limits the mechanical loading and hence strength requirements for the thin membrane material.

A few more elements are required to finish synthesizing a feasible ballute aerocapture solution. Recognizing that large ballutes will be needed to reduce heating, it becomes essential to use lightweight membrane material to limit the ballute mass. Practically speaking, this precludes the use of ablative materials and requires that ballute envelopes self cool by thermal radiation. The magnitude of this self-cooling, \dot{Q} , can be computed from the standard equation:

$$\dot{Q} = \sigma \varepsilon T^4 \quad (3)$$

where σ is the Stefan-Boltzman constant, ε is the material emissivity and T is the surface temperature. The temperature limit of the material therefore sets the maximum allowable self cooling rate which in turn dictates the required ballute size stemming from Equations 1 and 2. As shown in References 8-10, the resulting ballute sizes are on the order of 10-100 meters in diameter depending on the mission, sizes that dwarf the parent spacecraft in every case. It is perhaps only a slight exaggeration to say that the spacecraft will be effectively drag-free if the ballute is discarded. This suggesting the intriguing possibility that an aerocapture ballute can fly a purely ballistic trajectory and achieve the desired aerocapture orbit by simply detaching the ballute once enough velocity has been lost during the atmospheric passage. The remaining spacecraft then flies essentially drag free in its initial aerocapture orbit.

In summary, these are the essential elements of the large, towed aerocapture ballute concept:

- A ballute much larger than the parent spacecraft drastically shifts the trajectory to higher altitudes where the density is very low.
- Large structures in low density flows experience much reduced heating to the point that flexible, balloon-like materials can survive.
- Low ballute masses can be achieved by using thin-film material that does not ablate but self cools by thermal radiation.

- The ballute flies a ballistic trajectory in which the only modulation is timing the moment of ballute detachment from the spacecraft.
- The ballute is towed behind the spacecraft to both facilitate easy detachment and to prevent interference with spacecraft functions like telecommunications and thermal management.

While plausible, this concept clearly requires substantial technology development to verify the key assumptions and quantify performance levels. This development work is underway at NASA with initial emphasis on ballute materials, aerothermodynamic simulations, shock tunnel testing and trajectory analysis. The trajectory analysis element constitutes the main topic of this paper, in which we seek to answer the critical question of whether or not detaching the ballute during aerocapture can robustly place the spacecraft into the desired orbit despite some level of error in approach navigation and atmosphere knowledge. In the course of this analysis we will also produce some insights into the temperature and mass requirements of aerocapture ballute systems.

TECHNICAL APPROACH

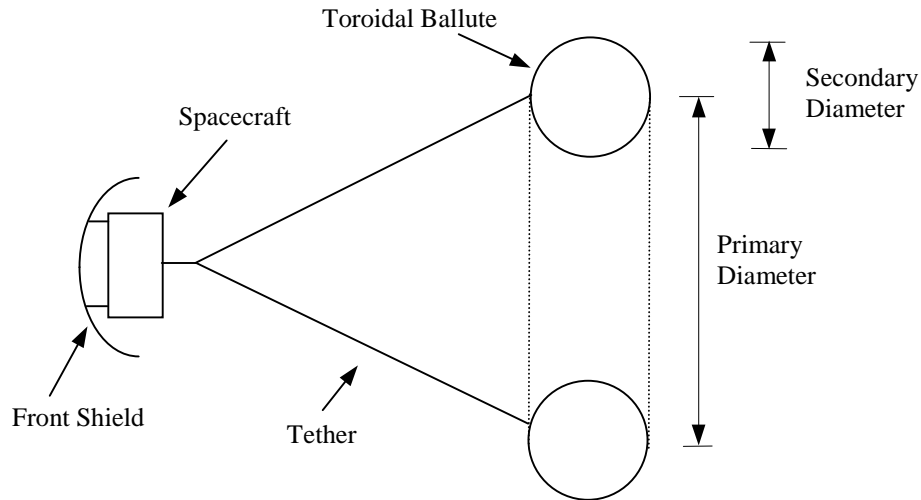
The trajectory analysis reported here takes the form of four case studies drawn from the missions listed in Table 1. The Titan Explorer, Neptune Orbiter and Venus Sample Return are major missions in the current NASA Space Science Strategic Plan,⁵ while the Mars Comm/Nav satellite represents a 100 kg class vehicle typical of piggyback or secondary payload missions. This set of four missions spans a large spectrum of the aerocapture parameter space: payloads from 100 to 2600 kg, entry speeds from 6.0 to 28.7 km/s, and atmosphere compositions of CO₂, N₂ or H₂/He.

Numerical simulations were performed for each mission using two different programs. The first program was BALLUTE_A/C, written and used by the lead author of this paper and based on the EES software package.¹¹ The second program was ACAPS, developed by the Naval Postgraduate School using the MATLAB software package and used by the second author of this paper.¹² Both programs were used to compute 2-D, non-lifting aerocapture trajectories at the target planets using inverse square gravity fields, non-rotating atmospheres, constant drag coefficients and atmospheric density profiles adapted from the open literature. These computations were set up as initial value problems in which the desired final orbits were found by iteration. Results from these two independent programs were cross-checked to ensure accuracy.

This study used a configuration depicted in Figure 1 where the spacecraft is protected on its forward surface by a 10 m radius of curvature spherical shield and tows a toroidal ballute behind it. Toroidal ballutes were chosen on the premise that this geometry can swallow the wake from the spacecraft and avoid fluid dynamic instabilities.¹³ The ballute shape actually does not matter from the trajectory analysis point of view because any vehicle with the same ballistic coefficient will fly the same trajectory. For this reason, the choice of 0.035 g/m² ballute envelope material is also not critical although it

determines the size of ballute needed to produce the desired ballistic coefficient. Heating estimates on the forward shield and trailing ballute stagnation points were made at every time step using Equation 2 where the proportionality constant, C , was derived from 2-D aerothermodynamic simulations of the flows using the NASA Langley LAURA computer program.¹⁴ Table 2 lists the physical constants, ballute properties, initial conditions and desired aerocapture orbits for each of the four missions computed here.

Figure 1: Aerocapture Vehicle Configuration



For each mission, the initial flight path angle, ϑ , was varied across a range to determine the allowable entry corridor given perfect approach navigation and atmospheric density profile knowledge. The only trajectory modulation variable involved was the time of ballute release during atmospheric flight. The shallow limit represents detaching the ballute essentially at the end of the atmospheric portion of the flight, while the steep limit represents a very early ballute release followed by a deep incursion into the atmosphere. The steep limit, in this sense, is restricted only by the allowable temperature experienced by the front shield during this deep descent. The resulting entry corridor widths must therefore be viewed as an ideal upper bound since the addition of navigation and atmospheric errors will reduce the widths. Neither BALLUTE_A/C nor ACAPS are set up to do proper Monte Carlo simulations with multiple error sources and so this work must await future investigations. Nevertheless, the ideal widths computed here can serve as a first order sanity check on the viability of ballistic aerocapture trajectories controlled by ballute detachment.

Table 2: Input Parameters for Aerocapture Calculations

	Titan Explorer	Neptune Orbiter	Venus Sample Return	Mars Comm/Nav
$m = GM \text{ (m}^3/\text{s}^2\text{)}$	9.142×10^{12}	6.871×10^{15}	3.249×10^{14}	4.283×10^{13}
Planet radius (km)	2575	24764	6052	3397
Atmospheric composition	98% N ₂ , 2% CH ₄	80% H ₂ 19% He 1% CH ₄	97% CO ₂ 3% N ₂	95% CO ₂ 3% N ₂ 2% Ar
Atmospheric density profile $\rho(h)$ (kg/m ³)	polynomial (Ref. 15)	$0.0013e^{-0.0168h}$ (Ref. 16)	$10^{-4} \times 10^{(99-h)/8}$ (Ref. 17)	$3.2 \times 10^{-5} \times e^{(60-h)/7.5}$ (Ref. 18)
Atmos. scale height (km)	53	60	3.5	7.5
non-ballute mass (kg)	325	230	2600	100
Ballute system mass (kg)	68	105	685	19
Ballute sys mass fraction	17%	31%	21%	16%
Ballute dimensions (m)	24 x 6 toroid	28 x 7 toroid	80 x 20 toroid	12 x 3 toroid
Ballute cross-sectional area (m ²)	450	615	5027	113
Ballute drag coefficient	1.39	1.51	1.31	1.45
Front shield area (m ²)	3	3	4	2
Ballistic coefficient (kg/m ²)	0.63	0.36	0.50	0.72
Shield stag. pt. heating coefficient (Eq. 2)	2.9×10^{-4}	7.9×10^{-5}	1.58×10^{-4}	2.63×10^{-4}
Ballute stag. pt. heating coefficient (Eq. 2)	1.92×10^{-4}	5.8×10^{-5}	1.07×10^{-4}	1.68×10^{-4}
Initial vehicle altitude (km)	1200	1200	200	125
Initial vehicle speed (m/s)	9600	28700	11600	6000
Apoapsis of aerocapture orbit (km)	1000	500000	300	600

RESULTS AND DISCUSSION

The BALLUTE_A/C and ACAPS calculations produced results in very close agreement to each other for all four missions. Sample outputs are shown in Figures 2 through 4 for Titan Explorer with an initial flight path angle of -34.1° . The altitude vs time (Fig. 2) and speed vs density (Fig. 3) plots show identical results between the two programs with a periapsis altitude of 529.1 km and a ballute detachment time of 368.2 s. Note the sharp corner in the lower right hand part of the speed vs density plot. This is the point of ballute detachment after which the speed changes little as the spacecraft climbs out of the atmosphere. The ballute stagnation point heating plot (Fig. 4) shows a relatively short duration pulse with a half width of roughly 120 s and a peak of 60000 W/m^2 at 160 s. The

spacecraft is inbound at this point at an altitude of 599 km. The density at this peak heating point is only $8.1 \times 10^{-7} \text{ kg/m}^3$, confirming the aforementioned very low density characteristic of aerocapture ballute trajectories. The peak heating corresponds to a maximum temperature of 1040 K assuming single-surface radiative self cooling with an 0.9 emissivity. Single surface radiative cooling is a conservative assumption because the ballute membrane will have some net energy flux away from the inside surface to the rest of the ballute; however, this effect has not yet been properly analyzed and quantified.

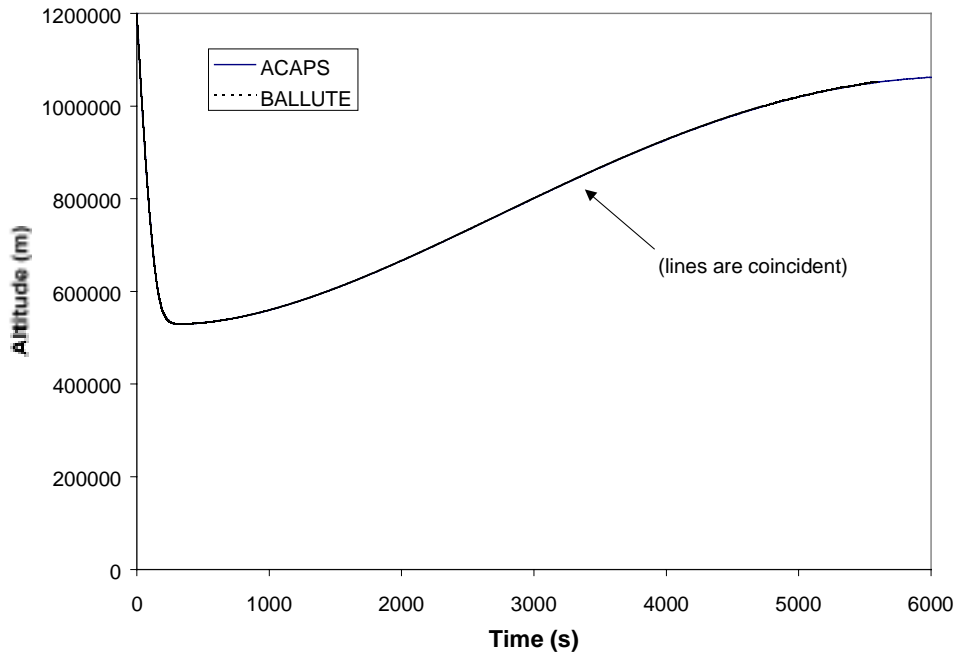


Figure 2: Titan Explorer Altitude vs Time Plot

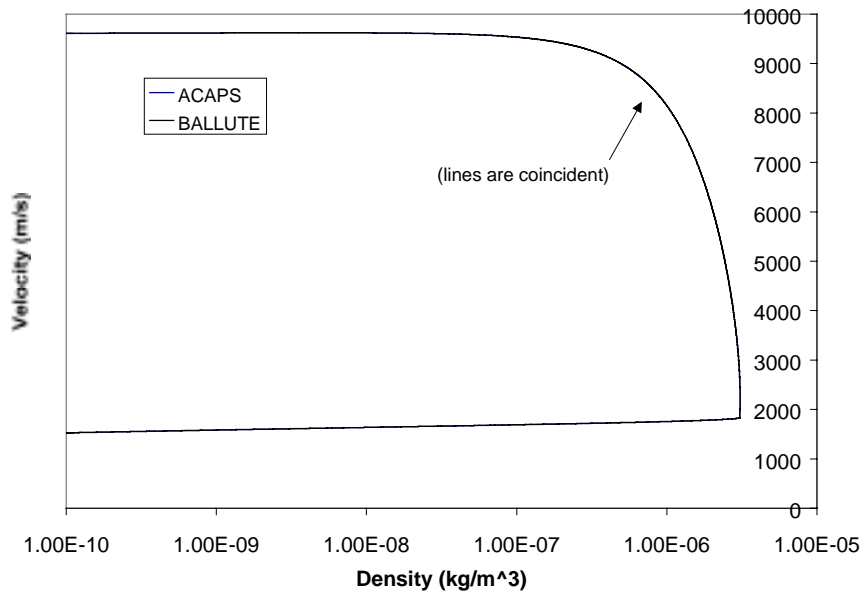


Figure 3: Titan Explorer Speed vs Density

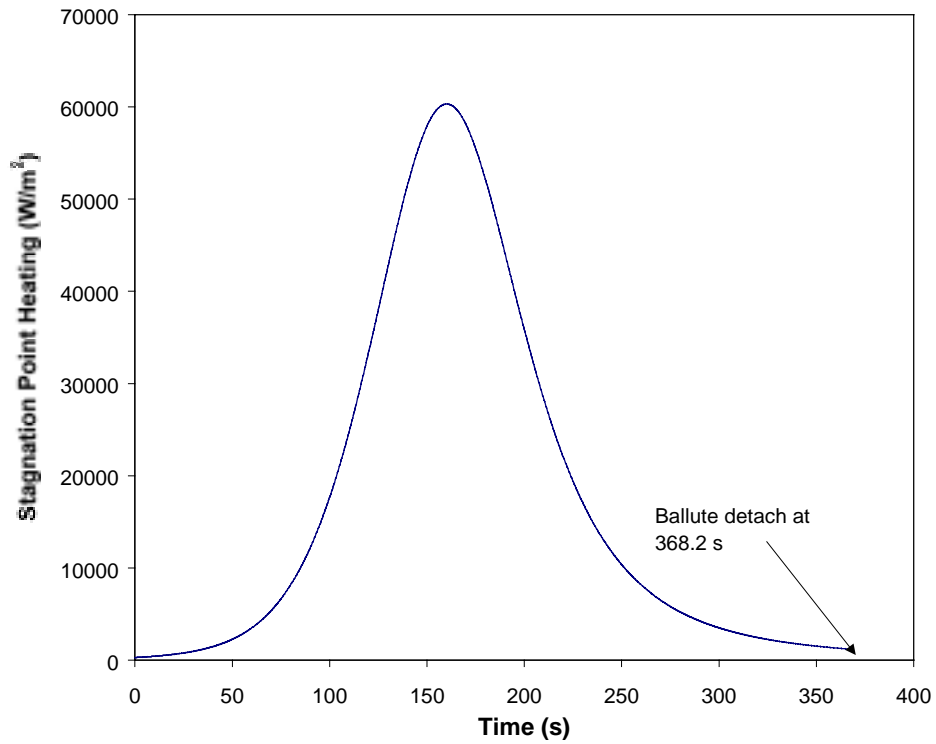


Figure 4: Titan Explorer Ballute Stagnation Point Heating Rate

Both BALLUTE_A/C and ACAPS were used to compute several Titan aerocapture trajectories across a range of initial flight path angles. The results are summarized in Figure 5. The plot shows the ballute apoapsis altitude after aerocapture as a function of the spacecraft speed at which the ballute was detached. The shallowest entry that yielded the desired apoapsis of 1000 km was $\vartheta = -33.5^\circ$. The steepest entry shown is $\vartheta = -36.0^\circ$, although even steeper entries would work if higher temperatures on the front shield were acceptable. The agreement between the two programs is seen to be very good. There is a general trend of greater sensitivity (higher slopes) at the steep end of the trajectory corridor reflecting the fact that ballute detachment on the inbound segment of the trajectory can more strongly influence the amount of atmosphere the parent spacecraft has to fly through compared to the outbound segment. The sensitivity can be quantified by considering the velocity error required to produce a 100 km apoapsis overshoot. At the shallow limit this velocity error is -20 m/s (outbound detachment delays give lower velocities and higher apoapses), while at the steep limit the velocity error is +6 m/s. These velocity errors equate to detachment time errors of 15 s at the shallow limit but only 0.2 s at the steep limit. This high sensitivity to ballute detachment time at the steep limit suggests that the onboard spacecraft avionics needs to be able to make detachment decisions on the order of 0.1 s. This short time result was also found to be true for the other missions.

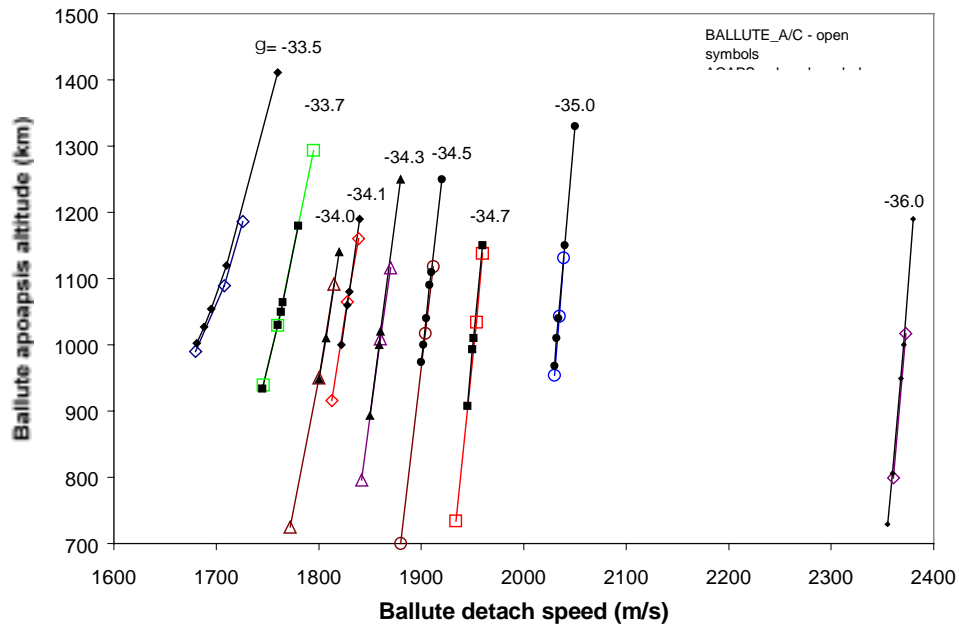


Figure 5: Titan Explorer Ballute Trajectory Corridor Results

Sample results from BALLUTE_A/C for all four missions are presented in Figures 6 and 7. Figure 6 shows the speed versus density plots for a selected initial flight path angle of each mission. The Titan curve is repeated from Figure 3 and illustrates the case where ballute detachment occurs very near the periapsis (minimum density). The Venus case is taken from the shallow entry limit in which the ballute is detached after periapsis in a region of appreciably higher density. In contrast, the Neptune and Mars cases have ballute detachment before periapsis and therefore show a density spike as the spacecraft continues into deeper atmosphere before moving out again. Despite these mission differences, the peak density experienced by the spacecraft remains very low in all cases.

Figure 7 shows the ballute stagnation point temperature as a function of time for the same missions depicted in Figure 6. The ballute is exposed to high temperatures for only a short period of time in every case. Indeed, from a heating point of view the entire aerocapture maneuver is completed within roughly 250 seconds at most, after which the ballute is discarded. Such short lifetimes make aerocapture ballutes very different from other kinds of inflatable structure or balloon applications in which operation for days or months is desired. One important consequence of this is that aerocapture ballutes will be much more tolerant of gas leaks through the membrane. In fact, given ballute sizes of 10+ meters and inflation pressures of only tens or hundreds of Pascals, it will be difficult to deflate the ballute within 250 seconds even with many large holes in the membrane. This suggests that aerocapture ballutes will be tolerant of localized burn-throughs and mechanical punctures, particularly near the stagnation point where internal and external pressures will be closely balanced.

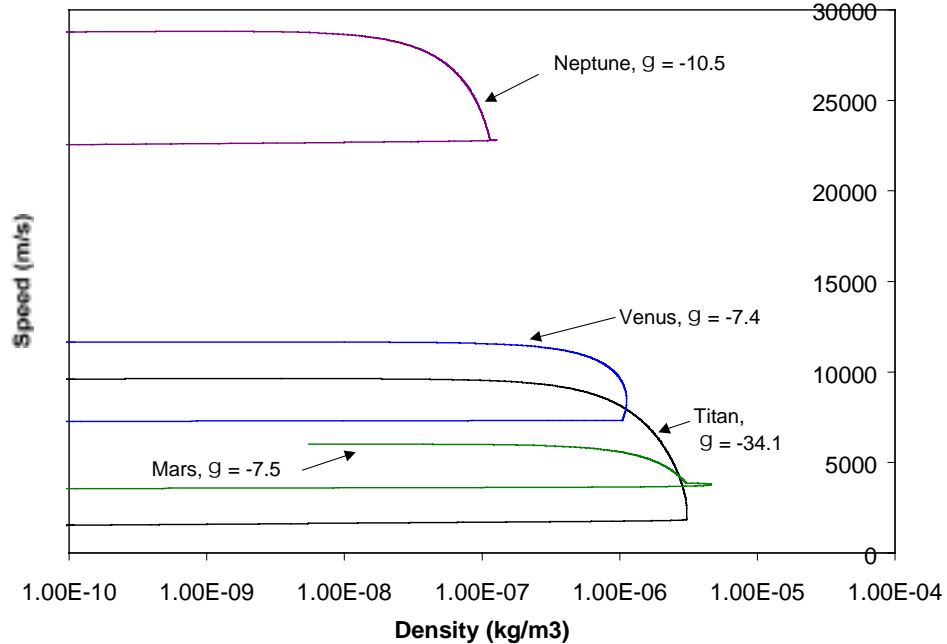


Figure 6: Sample Speed vs Density Plot For Each Mission

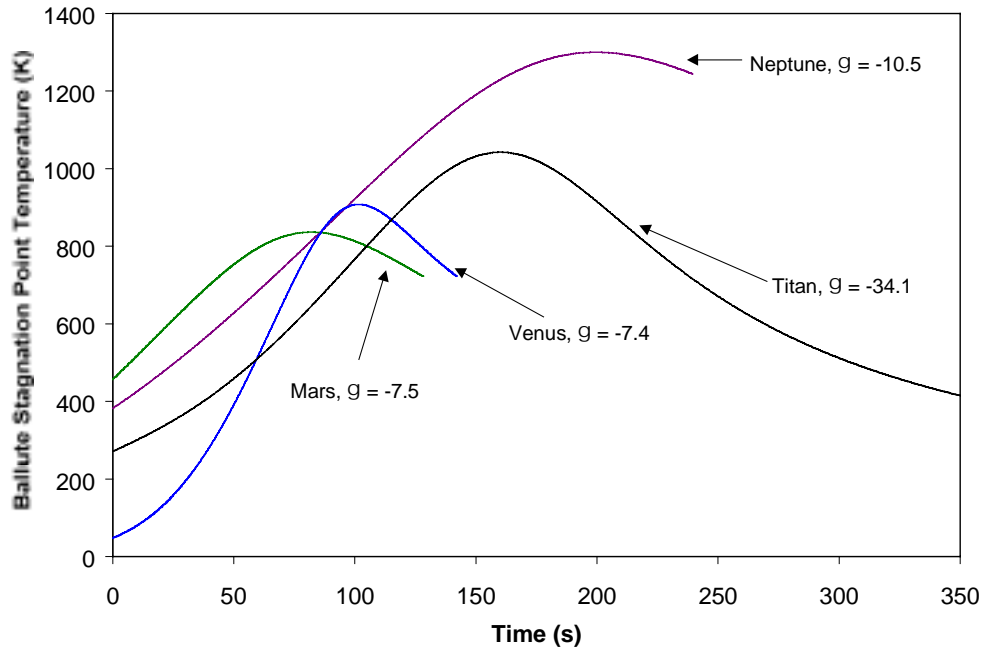


Figure 7: Sample Ballute Temperature Profiles For Each Mission

Trajectory corridor results for all four missions are summarized in Table 3. In each case the results were agreed upon by both the BALLUTE_A/C and ACAPS programs. The trajectory corridor limits are described in terms of both the initial flight path angle and the zero-drag periapsis altitude, which is the minimum altitude the spacecraft would reach given the initial flight path angle and the absence of drag. Quantifying the trajectory corridor in terms of this altitude range gives a first order estimate on the approach navigation accuracy required. For example, the Titan Explorer zero-drag altitude ranges from 459.6 km to 556.0 km, suggesting that the approach navigation requires a position accuracy of a small fraction of this 96.4 km span.

The four missions possess very different trajectory corridor widths. The Venus Sample Return mission has the smallest corridor, 0.3° or 7 km, while Titan Explorer has the largest corridor when measured by initial flight path angle, 2.5° , and Neptune Orbiter has the largest corridor when measured in distance, 123.5 km. The feature that unifies all of these missions is that the corridor distance divided by the density scale height of the atmosphere yields a common value of approximately 2. This suggests that the key parameter dictating the size of an aerocapture ballute trajectory corridor is atmospheric scale height, no matter what planet is involved.

Table 3: Summary of Aerocapture Ballute Trajectory Corridor Results

		Titan Explorer		Neptune Orbiter		Venus Sample Return		Mars Comm/Nav Sat	
		shallow limit	steep limit	shallow limit	steep limit	shallow limit	steep limit	shallow limit	steep limit
Width of ideal FPA corridor	deg	2.5		1.0		0.3		1.2	
Zero-drag periapsis range correspond. to FPA corridor	km	96.4		123.5		7.0		14.7	
Actual periapsis range	km	146.9		151.4		15.7		21.4	
Atmosphere scale height	km	53		60		3.5		7.5	
Zero-drag periapsis range / scale height		1.8		2.1		2.0		2.0	
Density ratio across actual periapsis altitude range		13.2		12.7		90.9		17.5	
		shallow limit	steep limit	shallow limit	steep limit	shallow limit	steep limit	shallow limit	steep limit
Initial flight path angle	deg	-33.5	-36.0	-10.2	-11.2	-7.4	-7.7	-7.00	-8.2
Zero-drag periapsis altitude	km	556.0	459.6	596.5	473.0	115.3	108.3	85.4	70.7
Detach time	s	666.0	241.0	283.8	191.8	142.0	99.9	256.7	88.9
Detach altitude	km	633.7	486.3	597.7	525.4	114.8	110.7	96.6	76.2
Detach speed	m/s	1680	2373	22734	23426	7316	8182	3610	4554
Post-aerocapture apoapsis	km	990	1017	482000	492370	298	340	590	578
Actual periapsis altitude	km	554.2	407.3	591.3	439.9	114.6	98.9	84.5	63.1
Density at actual periapsis	kg/m ³	1.9E-06	2.5E-05	6.3E-08	8.0E-07	1.1E-06	1.0E-04	1.2E-06	2.1E-05
Peak ballute temperature	K	1030	1073	1257	1369	908	974	805	868
Peak shield temperature	K	957	999	1196	1526	997	1485	707	864

The size of these ideal trajectory corridors would appear to be sufficient to accommodate the expected errors in approach navigation and atmospheric density profiles. For example, approach navigation on the Magellan mission to Venus provided errors of a couple of kilometers,¹⁹ a small fraction of the 15.7 km range computed for Venus Sample Return aerocapture. Improvements in spacecraft navigation techniques, particularly the development of onboard optical navigation, can be expected to further improve this situation. As far as atmospheric density profile errors are concerned, the two scale height corridor width suggests that uncertainties of the order of $\pm(1-e^{-1}) = \pm 63\%$ can be tolerated. This level of atmosphere knowledge would appear to be quite feasible for Mars given the wealth of data already accumulated by many spacecraft and the likelihood of other orbital assets when the aerocapture maneuver is performed. In contrast to Mars, however, knowledge for the other planets is not so extensive and it is less clear that the $\pm 63\%$ target can definitely be achieved. This issue requires further investigation, and it may turn out to be necessary for the spacecraft to carry instrumentation to measure the atmospheric density profile upon approach and provide last-minute information for the aerocapture maneuver.

In all of these calculations, the steep limit of the entry corridor is somewhat arbitrary. As mentioned previously, the practical limitation on even steeper trajectories is intolerably high heating rates on the ballute and/or forward spacecraft shield. The temperature limits listed in Table 3 (and illustrated graphically in Fig. 7) were chosen to represent what is or what may be achievable with ballute material technology. For example, the Mars Comm/Nav Sat temperature of 868 K on the ballute roughly corresponds to the temperature limit of polymer-based (PBO) balloon materials.²⁰ The selection of higher temperatures for the other missions, especially the 1300+ K limit for the Neptune Orbiter, will require ceramic, carbon or metal based materials. If lower temperature limits become necessary due to material development problems, then the ballute sizes will have to grow to compensate. In practice, however, there is a weak dependence of temperature on ballute size ($T \sim \dot{Q}^{0.25} \sim R_{cur}^{-0.125}$, i.e, Eqs. 2 and 3) which means that ballute masses grow quickly for only small decreases in temperature. This puts a premium on high temperature material development, and especially for high velocity missions like Neptune Orbiter.

The Venus Sample Return and Neptune Orbiter results show that the peak shield temperature becomes much greater than the peak ballute temperature at the steep trajectory limit. This reflects the fact that the ballute is detached rather early on the inbound leg of flight whereas the shield and spacecraft descend into much deeper atmosphere. This does not appear to be a problem given that the shield can be constructed from standard high temperature materials and that the miniscule dynamic pressure loading should enable very lightweight construction. However, as CNES found out with their Mars aerocapture aeroshell vehicle, there are difficulties with predicting separated flow off the edges of front shields and the possible interactions with downstream components. These issues clearly requires more work to complete front shield designs for this application. Nevertheless, the need for a front shield is clear based on the high temperatures generated by steep descents of these aerocapture ballute vehicles. It is simply not possible to protect the forward-facing spacecraft surfaces at these temperatures, even though use of high temperature multilayer insulation blankets.

CONCLUSION

Calculations for four different planetary missions have shown that significant trajectory corridors exist for large, towed aerocapture ballutes using only the time of ballute detachment as a modulation variable. Two independent computer programs were used to generate and cross-check the results. It appears that the computed corridor widths are sufficient to accommodate the anticipated approach navigation and atmospheric density profile errors for these missions; however, more work needs to be done to verify this. Although the absolute size of the corridor varies from mission to mission, the corridor size divided by the density scale height of the atmosphere was shown to yield a common value of approximately 2 despite a wide range of entry velocities and spacecraft sizes. The steep limit of the corridor is a function of the maximum allowable ballute

temperature rather than the ability to reach the desired aerocapture orbit; therefore, substantial advances in ballute materials technology will produce an ancillary benefit of wider trajectory corridors. Finally, the calculations revealed that the duration of ballute heating was less than 250 seconds for even the most challenging mission, Neptune Orbiter. This duration is so short as to render aerocapture ballutes relatively insensitive to gas leakage through holes in the membrane, especially in the high temperature stagnation point region where internal and external pressures are closely matched.

ACKNOWLEDGEMENTS

The authors would like to acknowledge helpful discussions and support from Angus McDonald, Andre Yavrouian and Jim Cutts of JPL, Hans Hornung of Caltech and Peter Gnoffo of NASA Langley. This work was jointly funded by the Mars and Deep Space Exploration Technology Programs at the Jet Propulsion Laboratory, California Institute of Technology, under a contract with the National Aeronautics and Space Administration.

REFERENCES

- ¹ Flatau, A., Olson, D. N. and Miller, M.C., "The Use of an Attached Inflatable Decelerator for Store Delivery From High Speed Aircraft From Low Altitude", AIAA 70-1199, presented at the AIAA Deceleration Systems Conference, Dayton, OH, Sept. 14-16, 1970.
- ² Iannotta, B., "Down-to-earth transport for space cargo", Aerospace America, July 2000, p. 39.
- ³ Bohon, H. L., Sawyer, J. W. and Miserentino, R., "Deployment and Performance Characteristics of 1.5-Meter Supersonic Attached Inflatable Decelerators", NASA-TN-D-7550, 1974.
- ⁴ Hall, J. L., "A Review of Ballute Technology For Planetary Aerocapture", Presented at the 4th IAA Conference on Low Cost Planetary Missions, Laurel, MD, May 2-5, 2000.
- ⁵ <http://sse.jpl.nasa.gov/roadmap/>
- ⁶ Dick Powell, NASA Langley, private communication, 2000.
- ⁷ Thien Lam-Trong, CNES, private communication, 2000.
- ⁸ McDonald, A., "A Light-weight Inflatable Hypersonic Drag Device For Planetary Entry", presented at the Association Aeronautique de France Conference at Arcachon, France, March 16-18, 1999.
- ⁹ McDonald, A., "A Lightweight Inflatable Hypersonic Drag Device For Venus Entry", AAS 99-355, presented at the AAS/AIAA Astrodynamics Specialist Conference, Girdwood, AK, August 16-19, 1999.
- ¹⁰ McDonald, A., "A Light-Weight Hypersonic Inflatable Drag Device For a Neptune Orbiter", AAS 00-170, presented at the AAS/AIAA Space Flight Mechanics Meeting, Clearwater, FL, January 23-26, 2000.
- ¹¹ Klein, S. A. and Alvarado, F. L. "Engineering Equation Solver", Version 5.180, F-Chart Software, 1999.
- ¹² Kan, J. Y. C., "Simulation of Aeroassisted Maneuvers in the Martian Atmosphere", M.S. Thesis, Naval Postgraduate School, Monterey, CA., Sept. 1999.
- ¹³ Rasheed, A., Fujii, K., Valiferdowski, B., and Hornung, H. G., (2000). "Preliminary Experimental Investigation of the Flow over a Toriodal Ballute", GALCIT Report FM 00-4, California Institute of Technology, July 7, 2000.
- ¹⁴ Gnoffo, P. A. "Computational Aerothermodynamics in Aeroassist Applications", to be presented at the 15th AIAA Computational Fluid Dynamics Conference, Anaheim, CA, June 11-14, 2001.
- ¹⁵ $\log_{10}(p)=A+Bh+Ch^2+Dh^3+ Eh^4 +Fh^5$, with $A=0.778687$, $B=-0.029026$, $C=7.3195e-5$, $D=-1.12923e-7$, $E=7.81597e-11$, $F=-1.98452e-14$, with h the altitude in km. From R. D. Lorenz, "Post-Cassini Exploration of Titan: Science Rationale and Mission Concepts", Appendix A.3, *JBIS*, Vol 53, No. 7/8, 2000.
- ¹⁶ adapted from James Bishop *et al*, "The Middle and Upper Atmosphere of Neptune", pp 427+ in *Neptune and Triton*, Dale P. Cruikshank, ed., Univ. of Arizona Press, Tuscon, 1995.

¹⁷ adapted from A. Sieff, "Thermal Structure of the Atmosphere of Venus", Ch. 11 in *Venus*, D. M. Hunten *et al.*, eds., Univ. of Arizona Press, Tuscon, 1983.

¹⁸ adapted from A. Sieff, "Models for the Martian Atmosphere", pp 3+ in *Advances in Space Research: The Mars Reference Atmosphere*, A. Kliore, ed., COSPAR-Pergamon Press, Oxford, UK, 1982.

¹⁹ Ted Sweetser, JPL, private communication, 2000.

²⁰ Andre Yavrouian, JPL, unpublished data, 2000.